Apatite in Blue Sapphire

One of the beauties of working with gemstones is that each time you peer into a stone, you get a glimpse of the universe held within. When we first examined the scene from figure 1 in a star sapphire, we were delighted with the view. A feature that immediately stands out is the triangular crystal, which displays terraced growth features and iridescence on the surface when illuminated with a fiber-optic light. Analysis with micro Raman revealed that this crystal is apatite.

What makes the scene even more stunning is the way the crystal seems to float over a cloud of rutile silk. This same silk is what creates asterism in the stone.

While in this case the apatite crystal resides in a sapphire from Sri Lanka, apatite has also been reported in corundum from a variety of sources, including Afghanistan, Cambodia, Madagascar, Myanmar, Nigeria, Pakistan, Tanzania, Thailand, the United States, and Vietnam.

Apatite can be found not only in ruby and sapphire from different origins, but also in many other types of gems. In our laboratory, we have encountered apatite inclusions in emerald, spinel, and garnet.

Apatite is a relatively common mineral, so it is not surprising to find it so often as an inclusion. Although it may occur frequently, in this instance it is anything but mundane.

E. Billie Hughes
Lotus Gemology, Bangkok

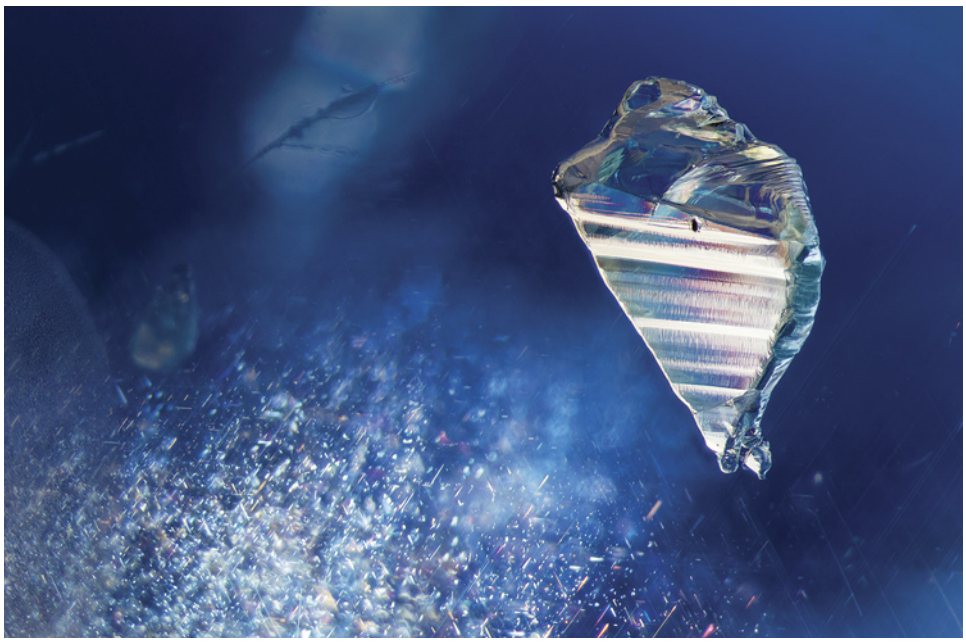

Figure 1. An apatite crystal is suspended over a cloud of rutile silk in this untreated star sapphire. Photomicrograph by E. Billie Hughes; field of view 6 mm.

Figure 2. This natural 2.01 ct Fancy Light brownish greenish yellow diamond octahedron was faceted to highlight an octahedral-shaped cloud inclusion. Photo by Nathan Renfro.

Faceted Octahedral Diamond with Octahedral-Shaped Inclusion

Recently, the authors examined a 2.01 ct faceted diamond octahedron (6.28 × 5.98 × 7.14 mm) with a Fancy Light brownish greenish yellow color grade that showed a distinctive internal appearance (figure 2). Microscopic examination revealed an octahedral-shaped inclusion scene composed of minute inclusions and clouds. The faceting arrangement of the diamond was likely meant to highlight the octahedron. Viewed from one perspective, the hexagonal facet shows the internal octahedron in such a way that the inclusion scene resembles a six-pointed star (e.g., figure 3; see the video at https://www.gia.edu/gems-gemology/fall-2021-microworld-diamond-octahedral-inclusion). Similar octahedral-shaped inclusions have been encountered before in natural diamonds (Winter 2015 Lab Notes, pp. 428–429; Spring 2011 Lab Notes, pp. 50–52).

Oftentimes, such symmetrical clouds are dark-colored or gray (W. Wang and W. Mayerson, "Symmetrical clouds in diamond—The hydrogen connection," *Journal of Gemmology*, Vol. 28, No. 3, 2002, pp. 143–152). These can also

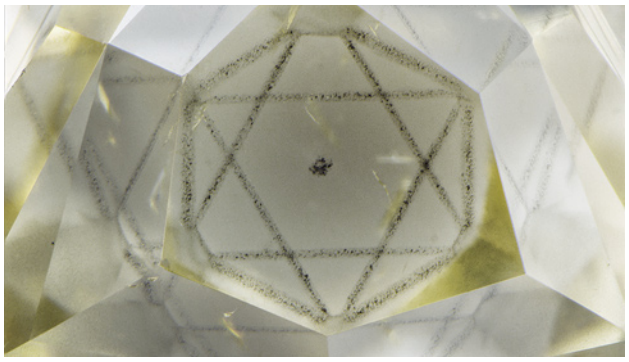

Figure 3. The faceting pattern for this diamond includes four hexagonal facets that provide a window of the octahedral-shaped inclusion. From this viewing angle, the octahedron resembles a six-pointed star. Photomicrograph by Nathan Renfro; field of view 4.69 mm.

contain evidence of hydrogen, nickel-related defects, or graphite (S. Eaton-Magaña et al., "Inclusion and point defect characteristics of Marange," *Diamond and Related Materials*, Vol. 71, 2016, pp. 20–29). At higher magnification, the individual inclusions that combine to create the cloud can be seen (figure 4).

The cloud inclusion resulted in an SI_1 clarity grade. The diamond exhibited no fluorescence to long-wave UV and blue N3-related fluorescence within the diamond when ex-

Figure 4. This detail of one of the octahedron's vertices indicates that the cloud comprises small inclusions. The portion of the octahedral cloud closest to the vertex within this image has a depth of approximately 1.8 mm below the hexagonal-shaped facet. Photomicrograph by Sally Eaton-Magaña; field of view 1.50 mm.

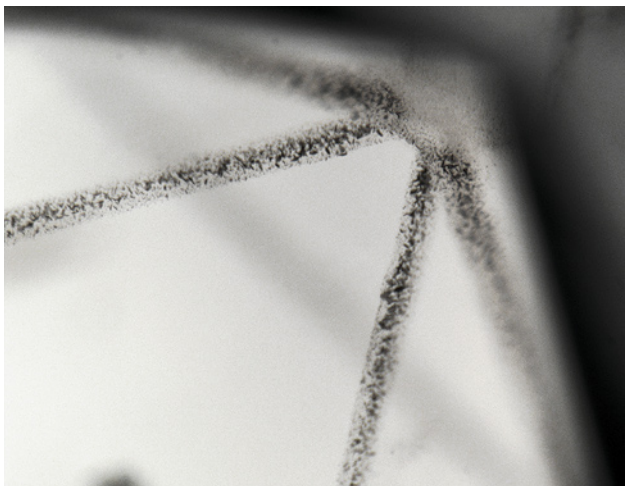

About the banner: This sunstone from Tanzania contains numerous platelets of hematite that are responsible for the aventurescence in this phenomenal gem. Photomicrograph by Nathan Renfro; field of view approximately 5 mm.

Gems & Gemology, Vol. 57, No. 3, pp. 268–275.

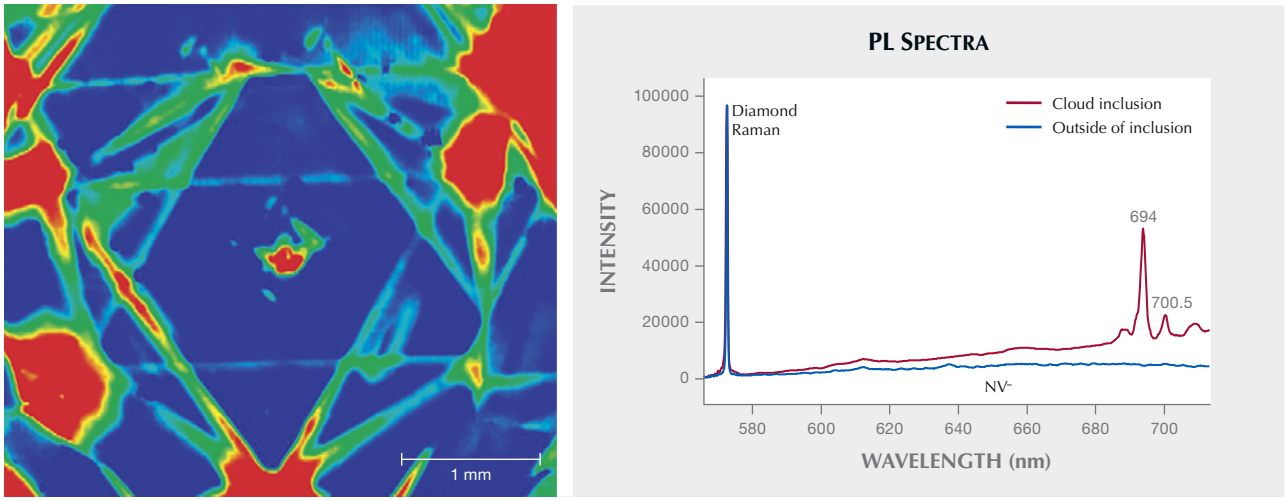

Figure 5. Left: This false-color PL map was compiled from thousands of spectra (each pixel is 15 microns in size) and plots the intensity of a peak centered at 694 nm (associated with nickel and often seen in hydrogen clouds). The detection of this peak corresponds well with the hydrogen cloud. The data were collected with 532 nm excitation at liquid nitrogen temperature, and the peak intensity is normalized by ratioing to the diamond Raman peak. Right: These two spectra were collected from a "red" and "blue" portion of the PL map. The diamond Raman areas are scaled equally. The cloud inclusions indicated elevated concentrations of peaks that include those at 694 and 700.5 nm; outside of the inclusion, there are increased concentrations of NV^- at 637 nm.

posed to the deep UV within the DiamondView. The cloud inclusion itself showed no distinctive fluorescence compared to the rest of the diamond. The IR absorption spectrum indicated the presence of strong nitrogen aggregates and a strong hydrogen peak at 3107 cm^{-1} associated with the N_3VH defect. The visible/near-infrared absorption spectrum contained typical cape features and a hydrogen-related band at 835 nm. The hydrogen features detected in the IR and Vis-NIR absorption spectra correspond with the presence of the octahedral cloud inclusion.

Spectroscopically, the most interesting results came from photoluminescence (PL) mapping of the octahedral-shaped cloud inclusion. This was performed at liquid nitrogen temperature using 532 and 455 nm excitations. Using 532 nm excitation, we saw elevated concentrations of peaks at 694 and 700.5 nm within the cloud inclusion (figure 5). The elevated concentrations of these peaks are consistent with previously characterized hydrogen clouds (e.g., Fall 2020 Lab Notes, pp. 416–419). The 694 and 700.5 nm peaks are ascribed to nickel and are often seen in hydrogen-rich diamonds (K. Iakoubovskii and G.J. Adriaenssens, "Optical characterization of natural Argyle diamonds," *Diamond and Related Materials*, Vol. 11, No. 1, 2002, pp. 125–131). In the 455 nm PL mapping, a nickel-nitrogen-related defect at 496.7 nm called the S3 center (T. Hainschwang et al., "The Rhodesian Star: An exceptional asteriated diamond," *Journal of Gemmology*, Vol. 34, No. 4, 2014, pp. 306–315) was also detected within the cloud. Outside of the inclusion, we detected higher concentrations of the NV^- defect (principal emission at 637 nm).

While the faceting pattern dramatically highlights the octahedral-shaped inclusion to resemble a six-pointed star, the cloud is not confined to a narrow focal plane as it might appear in figures 2 and 3. Instead, the cloud spans throughout much of the volume of the faceted stone. Creative faceting by the polisher provides a unique perspective on the cloud inclusion that makes this unusual diamond even more memorable.

Sally Eaton-Magaña and Nathan Renfro
GIA, Carlsbad

Alpesh Vavadiya
GIA, Mumbai

Hematite "Rose" Inclusion in Aquamarine

Recently, a 23.67 ct pear cabochon aquamarine with light greenish blue color and poor clarity was sent to the Taiwan Union Lab of Gem Research (TULAB) for identification. Microscopic observation of this aquamarine from the basal direction showed a number of negative crystals and black to brown hematite, confirmed by Raman spectroscopy. Hematite inclusions in gems usually appear in shapes such as flaky, striped, dendritic, or filamentous. Yet the hematite inclusions in this aquamarine seem to resemble a rose blossom composed of mathematical fractals (figure 6). It is worth mentioning that the rose form of hematite is common in hand specimens but rarely seen as inclusions. Photomicrography with brightfield illumination reveals this unique inclusion that shares a dash of science and romance.

Shu-Hong Lin
Institute of Earth Sciences,
National Taiwan Ocean University
Taiwan Union Lab of Gem Research, Taipei

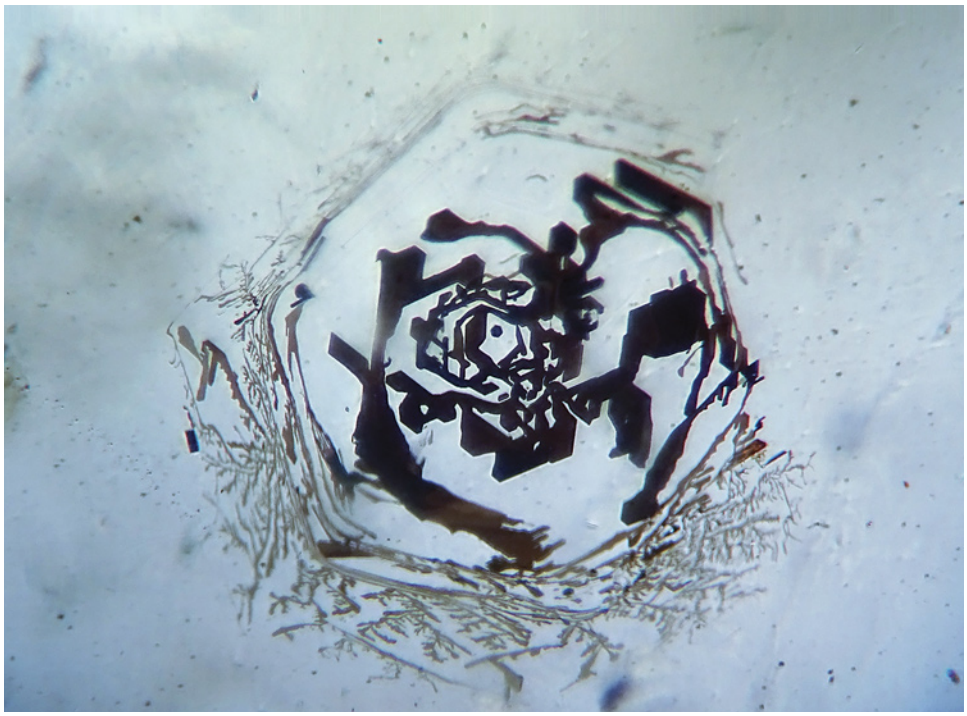

Figure 6. The aquamarine cabochon showed a fractal-like hematite inclusion with the beautiful outline of a rose. Photomicrograph by Shu-Hong Lin; field of view 0.64 mm.

Parisite Crystals in a Colombian Emerald

The author recently examined a 1.21 ct transparent faceted emerald. Gemological observation and chemical and spectroscopic analysis indicated that this natural emerald originated from Colombia. Moreover, microscopic examination with a combination of oblique fiber-optic and darkfield illumination presented the classic jigsaw pattern with a three-phase inclusion; this type of primary fluid inclusion is relatively common in Colombian emeralds. Interestingly, oblique fiber-optic illumination detected some colorless transparent crystal inclusions surrounded by fluid, as seen in figure 7.

Figure 7. Parisite crystals in an emerald from Colombia, shown under oblique fiber-optic illumination. Photomicrograph by Kyaw Thu; field of view 0.125 mm.

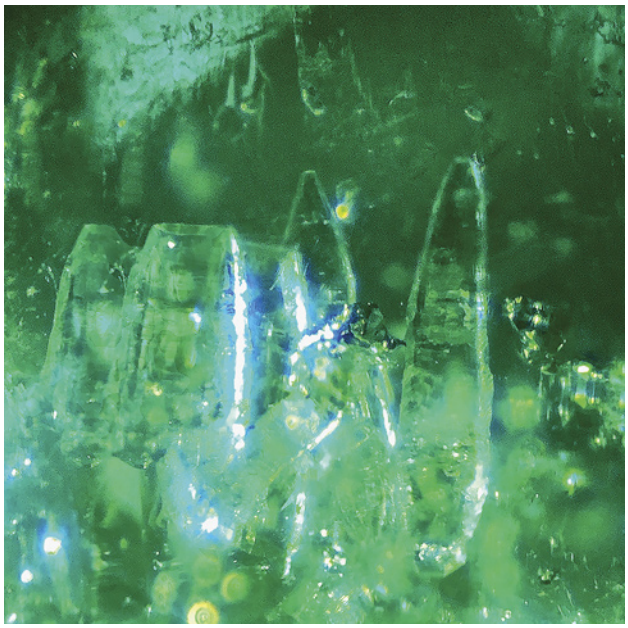

Raman microspectrometry analysis of the well-formed prismatic crystals indicated that the unusual fluorocarbonate minerals were parisite. These very rare parisite mineral inclusions have been found only in emeralds from the Muzo mine (Winter 1982 Lab Notes, p. 230; E.J. Gübelin and J.I. Koivula, *Photoatlas of Inclusions in Gemstones*, Vols. 1–3).

Kyaw Thu
S Gemmological Institute
Yangon, Myanmar

Iridescent Botryoidal Growth in Untreated Akoya Pearl

Cultured akoya pearls (*Pinctada fucata*) are typically admired for their high luster and desirable overtone. Nearly all pearls from this species undergo color treatment before entering the market. One untreated akoya pearl examined by the author exhibited an iridescent and botryoidal subsurface appearance when viewed with a fiber-optic light under microscopic magnification (figure 8). This was in sharp contrast to the pearl's appearance without magnification, which showed a light gray bodycolor and smooth surface.

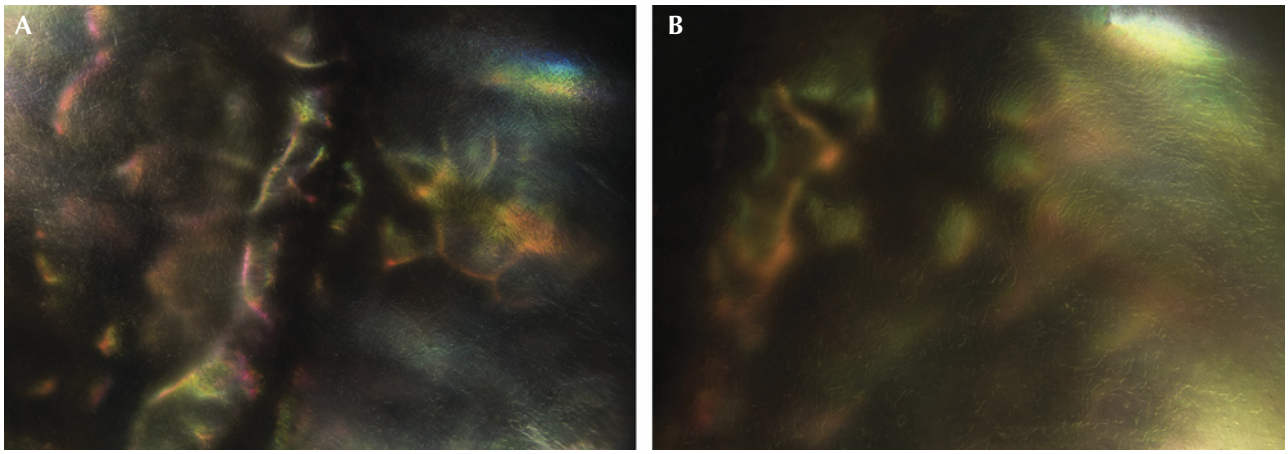

Figure 8. Iridescent and botryoidal subsurface growth seen in a pair of untreated akoya pearls. Note the nacre lines visible at the surface (top right of image B), giving context to the unusual growth and phenomenon below the surface. Photomicrographs by Britni LeCroy; field of view 3.57 (A) and 2.34 mm (B).

The light gray bodycolor of the pearl was caused by large voids or gaps surrounding its bead nucleus, which could be seen using real-time X-ray microradiography (RTX). Akoya pearls possess very thin nacre platelets that are transparent to translucent when viewed under strong lighting, allowing the viewer to see into the deeper layers of the pearl. The strong iridescence was caused by light interference within alternating layers of aragonite and conchiolin—the two substances that create nacreous pearls and that also have different refractive indices. Specifically, this iridescence is caused when incoming overhead light is reflected from the surfaces between the successive aragonite and conchiolin layers. When the reflected light rays from a bottom layer of nacre interfere with the incoming light, iridescence is created. In pearls, this feature is known as orient (E. Fritsch and G.R. Rossman, "An updated on color in gems. Part 3: Colors caused by band gaps and physical phenomena," Summer 1988 *G&G*, pp. 81–102). The underlying botryoidal structure combined with the iridescence from the overlying nacre was responsible for the unusual pattern or orient seen in this akoya pearl. This is the first time the author has encountered such a phenomenon in a pearl.

Britni LeCroy
GIA, Carlsbad

Fascinating Fluid Inclusions in Chinese Ruby

Gem rubies from the Yuanjiang deposit in Yunnan Province, China, host mineral inclusion assemblages com-

Figure 9. Fluid inclusion mimicking a snake in Yuanjiang ruby from China (left). The diagram on the right shows the details of this "snake." Photomicrograph by Wenqing Huang; field of view 0.26 mm.

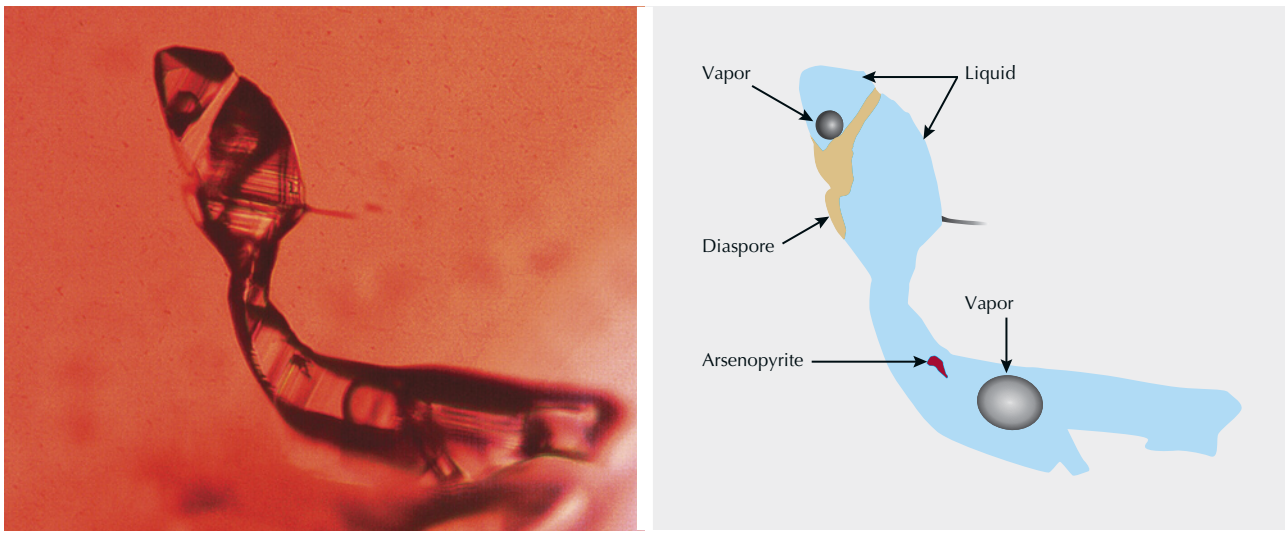

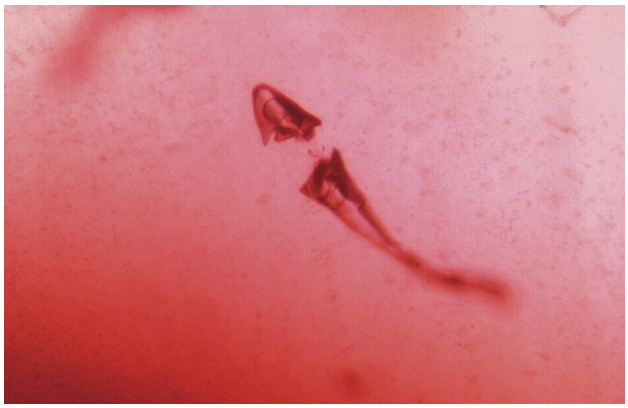

Figure 10. This Yuanjiang ruby from China contains an interesting fish-like fluid inclusion. Photomicrograph by Wenqing Huang; field of view 0.17 mm.

parable with those in rubies from other marble-hosted deposits (W.Q. Huang et al., "Trace element geochemistry and mineral inclusions constraints on the petrogenesis of a marble–hosted ruby deposit in Yunnan Province, China," *Canadian Mineralogist*, Vol. 59, No. 2, 2021, pp. 381–408). Moreover, the fluid inclusion scenes in rubies from all of these deposits are also similar (G. Giuliani et al., "Fluid inclusions in ruby from Asian marble deposits: Genetic implications," *European Journal of Mineralogy*, Vol. 27, No. 3, 2015, pp. 393–404).

Two rubies from the Yuanjiang deposit showed several interesting fluid inclusions. The most impressive one strongly resembles a snake raising its head (figure 9). The other mimics a fish (figure 10). As shown in figures 9 and 10, the whole fluid cavity was split into two parts, both of which show a bubble. Raman spectroscopy analysis identified the transparent tabular crystals in the snake as diaspore (figure 9). The "snake" also hosted a solid inclusion of arsenopyrite (FeAsS); the needle on its head could not be characterized by Raman spectroscopy due to its fineness. The fluid composition was dominated by CO_2 with minor components such as H_2S, COS, and CH_4, as revealed by Raman spectra and microthermometry. How these special inclusions formed has been speculated elsewhere (W.Q. Huang, "Fluid inclusion and titanite U–Pb age constraints on the Yuanjiang ruby mineralization in the Ailao Shan–Red River metamorphic belt, southwest China," *Canadian Mineralogist*, 2021, accepted). This morphology-forming process has been explained by two mechanisms that evolved step by step. The first is morphological ripening that resulted in negative shapes of fluid inclusions; the second consists of subsequent reactions between the trapped H_2O and the host corundum during the cooling of the inclusion, generating a diaspore that segregated the fluid completely.

Inclusions (mostly mineral inclusions) in gemstones that mimic scenery and landscapes are fascinating and relatively common. One novelty inclusion, an interesting "fried egg" of epigenetic residue trapped in a fissure, was recently found in rock crystal quartz (Fall 2020 *G&G* Micro-World, pp. 430–431). However, such novelty inclusions, especially fluid inclusions mimicking animals, are exceptionally rare.

Wenqing Huang (67019822@qq.com)
National Center of Supervision and Inspection on Quality of Gold and Silver Products
Nanjing Institute of Product Quality Inspection
Nanjing, China

Tourmaline in Paraíba Tourmaline

The authors examined the 3.21 ct Paraíba tourmaline shown in figure 11. The stone was moderately included with fine thread-like trichite fluid inclusions, growth tubes, and many fractures. Growth tubes are often open on one or both ends and may contain epigenetic minerals encapsulated within such as limonite, cookeite, hematite, prosopite, and tourmaline (E.J. Gübelin and J.I. Koivula, *Photoatlas of Inclusions in Gemstones*, Vol. 2, pp. 763, 764, and 780–781). In this tourmaline, we observed a long prismatic crystal that had a morphology consistent with tourmaline, which was confirmed using Raman spectroscopy. This offered an interesting example of a gem tourmaline that contained a tourmaline inclusion.

Sudarat Saeseaw and Suwasan Wongchacree
GIA, Bangkok

Willemite in Topaz

The authors recently had the opportunity to examine a 28.61 ct transparent freeform custom-cut study block of colorless topaz (figure 12) from Jos in Plateau State, Nigeria, that hosted a very large forest green inclusion of chlorite with an intricate stepped surface structure. Magnification showed that the chlorite inclusion was partially rimmed by

Figure 11. A tourmaline inclusion in Brazilian Paraíba tourmaline. Photomicrograph by Suwasan Wongchacree; field of view 4.8 mm.

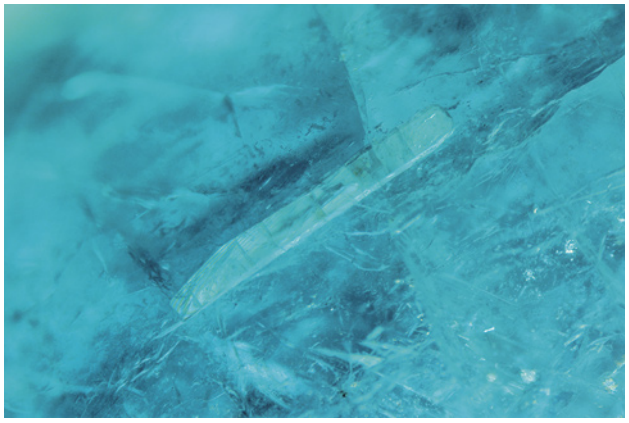

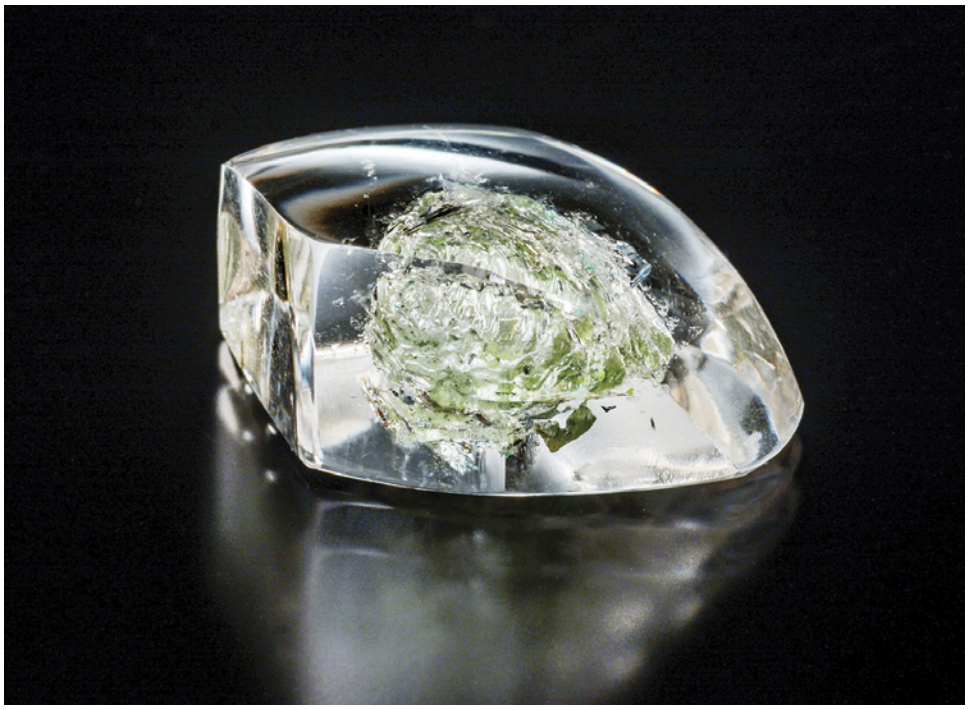

Figure 12. This 21.36 × 14.94 × 9.44 mm custom-cut study block of topaz from Jos, Nigeria, is host to several interesting inclusions. Photo by Diego Sanchez.

transparent near-colorless crystals (figure 13) identified by laser Raman microspectrometry as willemite (Zn_2SiO_4), a trigonal zinc silicate.

The willemite crystals in this topaz fluoresced bright yellow-green to short-wave ultraviolet radiation, giving the chlorite a partial fluorescent halo. This is the only known example of the mineral willemite as inclusions in topaz from any locality.

In addition to the willemite, bright bluish green patches of color on the chlorite might be the microcline feldspar amazonite, but Raman analysis could not identify them.

Figure 13. Transparent colorless willemite crystals appear to be tumbling down the slope of a large chlorite inclusion in a Nigerian topaz. Photomicrograph by Nathan Renfro; field of view 4.02 mm.

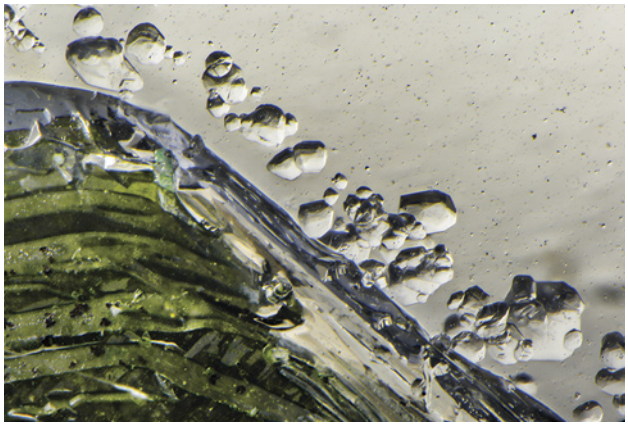

There were also some tiny rounded opaque inclusions with metallic luster that resembled metal sulfides. Bright red epigenetic hematite was found in one surface-reaching cleavage crack, and a few tiny transparent brownish yellow high-relief crystals of sphalerite were also present with the willemite.

John I. Koivula and Nathan Renfro
GIA, Carlsbad

Quarterly Crystal: Fibers and Rods in Euclase

From time to time in the laboratory, we run into problems that we just cannot resolve. Just such a situation was recently encountered when we examined a very unusual 10.82 ct transparent euhedral crystal of orange-pink euclase measuring 14.71 mm wide, pictured in figure 14. We knew from experience that the natural surface striations on this transparent crystal would make conclusive identification of the inclusions difficult at best. The euclase crystal, recently recovered during limited mining in Livramento de Nossa Senhora in Bahia, Brazil, was acquired from Luciana Barbosa of the Gemological Center in Asheville, North Carolina. The cause of the unusual padparadscha-like orange-pink color of this euclase production was determined to result from impurities of Mn^{3+} (L. Gilles-Guéry et al., "Mn^{3+} and the pink color of gem-quality euclase from northeast Brazil," accepted by *American Mineralogist*, 2021).

On examination with a gemological microscope, we observed fine branching fibers and rods of white to red-brown color suspended in the euclase (figure 15). The red-brown color of some of the inclusions suggested epigenetic alteration at some point. As shown in the photomicrograph

Figure 14. The orange-pink color of this 10.82 ct Brazilian euclase is reminiscent of padparadscha sapphire. Photo by Diego Sanchez.

in figure 16, we observed a tiny hollow cylindrical void containing a dark brown fluid and a mobile gas bubble. The color of the fluid made it difficult to clearly see the gas bubble, unless it was moving.

As we suspected, laser Raman microspectrometry could not pin down the identification of the inclusions. Raman testing only showed the peaks for the euclase host. We also tried energy-dispersive X-ray fluorescence (EDXRF) to pick up any hints of unusual chemistry, but again useful information eluded us. After several tries at both Raman and EDXRF, we finally realized that destructive analysis would be needed for a clear identification of the inclusions. Since this well-formed euclase crystal has a very rare and unusual color, we decided not to use destructive analysis. We would keep the euclase intact, to be enjoyed as a gem mineral specimen.

John I. Koivula and Nathan Renfro
Ian Nicastro
San Diego, California

Figure 15. Attempts to identify these acicular inclusions discovered in the 14.71 mm euclase crystal proved unsuccessful. Photomicrograph by Nathan Renfro; field of view 2.56 mm.

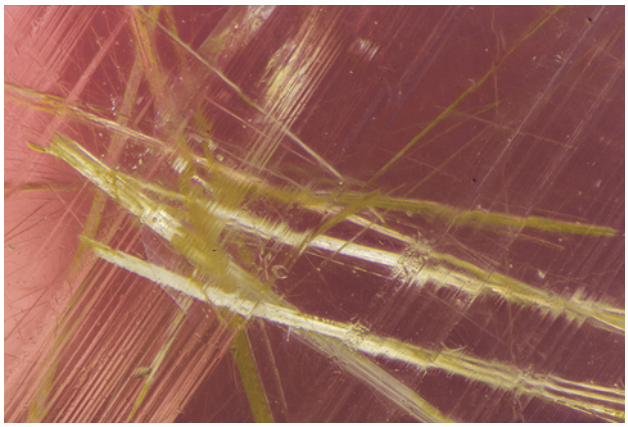

Figure 16. With a dark brown fluid and a moving bubble, this tiny cylindrical void was a surprising discovery. Photomicrograph by Nathan Renfro; field of view 0.288 mm.